Ann. Geophys., 26, 843–852, 2008
www.ann-geophys.net/26/843/2008/

Annales Geophysicae

Mapping ionospheric backscatter measured by the SuperDARN HF radars – Part 2: Assessing SuperDARN virtual height models

T. K. Yeoman[1], G. Chisham[2], L. J. Baddeley[1], R. S. Dhillon[1], T. J. T. Karhunen[1], T. R. Robinson[1], A. Senior[3], and D. M. Wright[1]

[1]Dept. of Physics and Astronomy, University of Leicester, University Road, Leicester, LE1 7RH, UK
[2]British Antarctic Survey, Natural Environment Research Council, High Cross, Madingley Road, Cambridge, CB3 0ET, UK
[3]Department of Communication Systems, Lancaster University, Lancaster, LA1 4WA, UK

Received: 20 August 2007 – Revised: 29 August 2007 – Accepted: 6 March 2008 – Published: 13 May 2008

Abstract. The Super Dual Auroral Radar Network (SuperDARN) network of HF coherent backscatter radars form a unique global diagnostic of large-scale ionospheric and magnetospheric dynamics in the Northern and Southern Hemispheres. Currently the ground projections of the HF radar returns are routinely determined by a simple rangefinding algorithm, which takes no account of the prevailing, or indeed the average, HF propagation conditions. This is in spite of the fact that both direct E- and F-region backscatter and $1\frac{1}{2}$-hop E- and F-region backscatter are commonly used in geophysical interpretation of the data. In a companion paper, Chisham et al. (2008) have suggested a new virtual height model for SuperDARN, based on average measured propagation paths. Over shorter propagation paths the existing rangefinding algorithm is adequate, but mapping errors become significant for longer paths where the roundness of the Earth becomes important, and a correct assumption of virtual height becomes more difficult. The SuperDARN radar at Hankasalmi has a propagation path to high power HF ionospheric modification facilities at both Tromsø on a $\frac{1}{2}$-hop path and SPEAR on a $1\frac{1}{2}$-hop path. The SuperDARN radar at Þykkvibær has propagation paths to both facilities over $1\frac{1}{2}$-hop paths. These paths provide an opportunity to quantitatively test the available SuperDARN virtual height models. It is also possible to use HF radar backscatter which has been artificially induced by the ionospheric heaters as an accurate calibration point for the Hankasalmi elevation angle of arrival data, providing a range correction algorithm for the SuperDARN radars which directly uses elevation angle. These developments enable the accurate mappings of the SuperDARN electric field measurements which are required for the growing number of multi-instrument studies of the Earth's ionosphere and magnetosphere.

Keywords. Ionosphere (Active experiments; Wave propagation; Instruments and techniques)

Correspondence to: T. K. Yeoman
(tim.yeoman@ion.le.ac.uk)

1 Introduction

The Super Dual Auroral Radar Network (SuperDARN) network (Greenwald et al., 1995; Chisham et al., 2007) currently consists of 11 over-the-horizon HF radars in the northern polar regions and 7 radars in the southern polar regions. Radars of this design have been in operation since the early 1980s, and currently form a powerful diagnostic of large-scale ionospheric and magnetospheric dynamics in the Northern and Southern Hemispheres. The radars operate between 8 and 20 MHz, and have fields-of-view which extend in range from 180 km to over 3000 km in standard operations. The radar systems rely on the refraction of the HF radiation both in order to achieve orthogonality to the Earth's magnetic field, a requirement for scattering off the ionospheric irregularities, which form the targets for such radar systems, and to achieve backscatter from the longer ranges, which require over-the-horizon operations. The ground locations of the HF radar returns are routinely determined by a simple rangefinding algorithm, which uses the group delay of the signal and an assumed virtual height to map the radar returns, assuming straight-line propagation at the speed of light (see the companion paper, Chisham et al., 2008, for a fuller discussion), and thus takes no direct account of the prevailing HF

Published by Copernicus Publications on behalf of the European Geosciences Union.

propagation conditions (Baker et al., 1986). In reality these propagation conditions are highly variable, with direct ($\frac{1}{2}$-hop) propagation to E- and F-region ionospheric irregularities, and $1\frac{1}{2}$-hop propagation to both the E- and F-region commonly observed by the radar systems.

A number of approaches are possible in order to improve the mapping of radar backscatter. In general the true height of radar echoes is not known. For naturally-occurring radar targets the virtual height appropriate to the unknown real irregularity height must be substituted by a model altitude, the pseudo-virtual height. Improvements to such model virtual heights formed the subject of Chisham et al. (2008). Alternatively, if radar measurements of the elevation angle are available, then a custom analysis of the HF propagation mode may be performed to directly determine the real height, and hence the echo location. A different approach is possible for backscatter generated by a high power RF facility, such as the data examined here, where the true height may be accurately determined via incoherent scatter radar data, the actual location of the scatter is known, and the effects of different methods of echo location may be investigated.

Previous studies of the mapping of HF radar backscatter have adopted a raytracing simulation (Villain et al., 1984; Baker et al., 1986) or velocity field cross correlation (Ruohoniemi et al., 1987; André et al., 1997) approach to assess the accuracy of rangefinding using the straight-line approximation. These studies suggested agreement between the ground range and radar range within ∼15 km over a $\frac{1}{2}$-hop path. Over such relatively short propagation paths, therefore, the existing rangefinding algorithm is clearly adequate. However mapping errors are expected to become more significant for longer paths where the roundness of the Earth becomes important, and a correct assumption of virtual height becomes more difficult.

Early studies with HF radars either used HF radar data alone, or combined HF radar data with data from instruments such as ground magnetometers, which had a limited spatial resolution and are often only available from arrays which are sparsely populated in comparison to radar fields-of-view. However the growing importance of combined ground-spacecraft measurements and multi-instrument studies from the ground have led to numerous coordinated studies with instruments of a high spatial resolution, such as meridian scanning photometers, all sky cameras and auroral imagers. In these studies the location of the radar backscatter is a crucial element in the study. In addition, spacecraft overpasses, where the magnetic conjugate points are computed to a high precision using geomagnetic field models, require high accuracy in the location of the HF radar backscatter. For example optical signatures associated with dayside reconnection have been extensively investigated from the ground in visible light at wavelengths of 630.0 nm and 557.7 nm associated with auroral activity (e.g. Sandholt et al., 1996) at a high spatial resolution. In association with these optical transients, HF radars observe pulsed ionospheric flows in the cusp region (e.g. Pinnock et al. 1995). Such radar and optical signatures may be observed simultaneously (Yeoman et al., 1997a), but the interpretation of such studies requires an accurate evaluation of radar range. A plethora of recent multi-instrument studies of, for example, convection reversal boundaries (e.g. Sotirelis et al., 2005), spectral width boundaries (e.g. Chisham et al., 2005), spacecraft conjunctions (e.g. McWilliams et al., 2004), high resolution ground-based auroral images (e.g. Lockwood et al., 2003) and incoherent scatter radar observations (e.g. Blanchard et al., 2003) all rely critically on an accurate evaluation of the true ground range of HF coherent backscatter returns, often over the long propagation paths where accurate mapping becomes more difficult. Yeoman et al. (2001) performed a preliminary evaluation of the absolute rangefinding accuracy of current routine analysis of the SuperDARN network of over-the-horizon HF radars comparing the ground range, calculated group path and measured radar slant range of backscatter artificially excited by the EISCAT heating facility at Tromsø. HF propagation over a $\frac{1}{2}$-hop path, a $1\frac{1}{2}$-hop path and a $2\frac{1}{2}$-hop path were examined. The radar slant range and the calculated group paths were found to be in excellent agreement for all three paths, with the standard algorithm for backscatter ground range location accurate to within 16 km and 114 km for $\frac{1}{2}$-hop and $1\frac{1}{2}$-hop backscatter, respectively, when using the true backscatter height. These range offsets were extremely consistent. The analysis of Yeoman et al. (2001) suggested that high elevation angle backscatter should be interpreted with caution.

In this paper HF radar backscatter which has been artificially-induced at a precisely known location by high power RF facilities at Tromsø and on Svalbard are used to provide a range accuracy evaluation for the SuperDARN radars. The location of the artificial irregularities is determined through the combination of the beam direction of the high power RF facilities and the ionospheric interaction height of the RF beam, as determined from collocated incoherent scatter radar measurements of the modified ionosphere. These propagation paths provide an opportunity to quantitatively test the available SuperDARN virtual height models as presented in Chisham et al. (2008) and highlight significant issues with the accuracy of the standard SuperDARN rangefinding algorithm. In addition, direct use of the measured elevation angle of arrival provides a new method of determining the backscatter location for $1\frac{1}{2}$-hop paths with elevation angles in the range 10°–30° for SuperDARN data recorded at ranges 1500–2500 km, where reliable elevation angle data exist.

2 Instrumentation

The data presented here result from the generation of HF coherent backscatter from artificial ionospheric irregularities in the fields-of-view of the SuperDARN radars at Hankasalmi

and Þykkvibær with the EISCAT heater at Tromsø (Rietveld et al., 1993) and SPEAR (Wright et al., 2000; Robinson et al., 2006), the new ionospheric modification facility on Svalbard. Details of SuperDARN are given in Greenwald et al. (1995) and Chisham et al. (2007). Figure 1 presents the beam and range locations for the 15 km range gate radar scan modes used in this study. For the SPEAR experiments, a restricted scan ran on both channels of the radar, one using 45 km range gates, starting at a range of 180 km and the other 15 km range gates, starting at 1485 km. A frequency sweep mode was employed, ranging from 9.9–13.3 MHz, using integration times of 1 or 2 s per beam. Here data for Þykkvibær beam 6 and Hankasalmi beam 9, which intersect over SPEAR, are presented. Experiments performed with the EISCAT Tromsø heating facility employed a similar scan pattern, with data from 15 km range gates starting at a range of 1470 km for Þykkvibær beam 15 and 15 km range gates starting at a range of 480 km for Hankasalmi beam 5 presented here, these beams intersecting over the Tromsø heater. In Fig. 1 range gates are marked every 10th gate. For the EISCAT Tromsø experiments the heater operated at 50% power (using 6×80 kW transmitters, an effective radiated power, ERP, of $\sim$130 MW), at a frequency of $\approx$4–5 MHz for 4-h intervals. For SPEAR experiments, the full SPEAR array was used (48×2 kW transmitters), providing an ERP of $\sim$15 MW, again between 4–5 MHz. The heaters produce artificial electron density irregularities in the F-region ionosphere (Robinson, 1989), which act as targets for the HF radars (Robinson et al., 1997; Yeoman et al., 1997b). The artificial targets result in very high returned backscatter power in comparison to naturally-occurring irregularities. This allows a short integration time to be run on the radar, providing higher time resolution than is normally available. Here backscatter power and elevation angle of arrival calculated from a cross correlation between signals detected on the main radar array and the interferometer array are used. The accuracy of these elevation angles has been verified through a detailed calibration of the angles measured at a wide range of frequencies over a $\frac{1}{2}$-hop Hankasalmi-Tromsø path (see the experiment described in Senior et al., 2004), and through a comparison of the data recorded with raytrace calculations through a model ionosphere constrained by measurements taken from the EISCAT dynasonde, close to the midpoint of the Hankasalmi–SPEAR propagation path. A schematic of $1\frac{1}{2}$-hop HF radar propagation paths to the ionosphere above the heating facilities is presented in Fig. 2. Here a raytrace of ray paths for a typical ionosphere are shown in red, illustrating the refraction of the HF rays as a consequence of the increasing electron density as altitude increases in the ionosphere. The radar elevation angle is the angle between these rays and the horizon at the radar site. Backscatter occurs where the HF rays intersect the region in which the heater pump wave generates striations in the ionospheric plasma. The straight blue line joins the radar location and the pseudo-virtual height – the virtual height which the SuperDARN rangefinding algorithm assumes is appropriate for the backscatter in order to deduce its ground range. The angle this blue line makes to the horizon at the radar site, α, is here referred to as the takeoff angle.

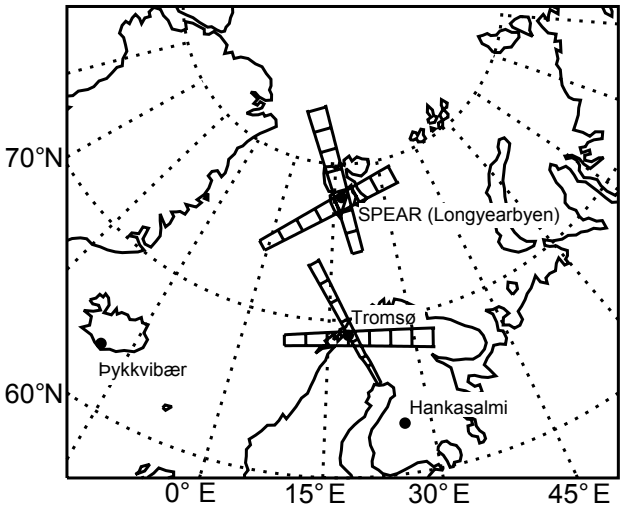

Fig. 1. Beam and range locations for the radar modes used in this study. Range gates are marked every 10th gate.

3 Observations

Figure 3 presents a range gate – time representation of backscatter power measured by the 45 km range gate channel of the Hankasalmi radar during a period of SPEAR high power operations on 17 April 2005. SPEAR O-mode operations are indicated by vertical black lines and red horizontal lines at the top and bottom of the panel. Intervals of strong backscatter centred on range gate 45 can be seen when SPEAR is transmitting. The continuous backscatter at range gates $\sim$30 is the ground scatter which supports this $1\frac{1}{2}$-hop propagation path. Initially a sequence of 4 min on, 4 min off O-mode transmissions were performed. Clear backscatter power signatures can be seen for each "on" cycle. At 17:20 UT a continuous 1 h O-mode transmission commenced. Strong backscatter was observed throughout this interval, apart from a small gap at $\sim$18:00 UT, when the critical frequency of the F-region above SPEAR dropped below the SPEAR transmit frequency of 4.45 MHz. Data originating from a known, fixed location such as those presented in Fig. 3 will now be used over a number of propagation paths, and with a number of virtual height models, in order to investigate the accuracy of the SuperDARN rangefinding algorithms.

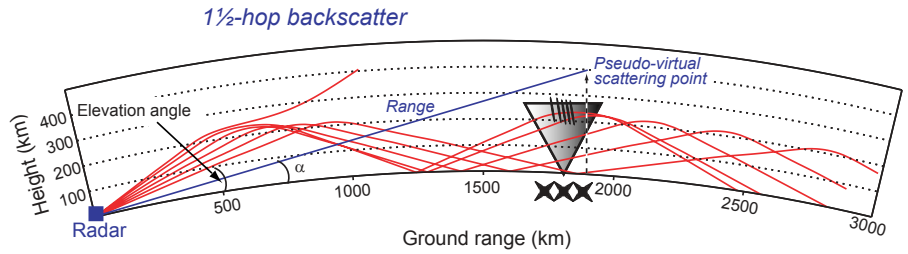

Fig. 2. A schematic of $1\frac{1}{2}$-hop HF radar propagation paths to the ionosphere above the Tromsø and SPEAR heating facilities.

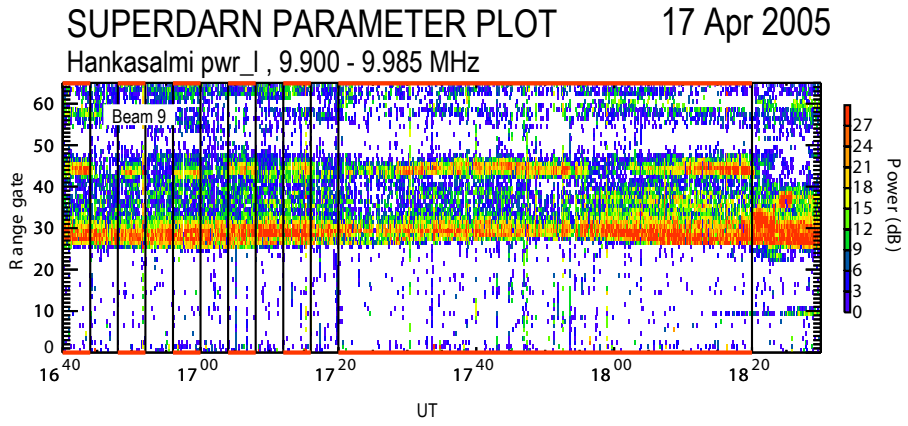

Fig. 3. (a) A range gate-time representation of backscatter power measured by the Hankasalmi radar during a period of SPEAR high power operations on 17 April 2005. Backscatter power is color-coded according to the bar to the right of the panel. SPEAR O-mode operations are indicated by vertical black lines and red horizontal lines at the top and bottom of the panel. Intervals of strong backscatter centred on range gate 45 can be seen when SPEAR is transmitting.

3.1 Evaluating the effect of virtual height models on rangefinding accuracy

In order to assess the overall performance and consistency of the radar rangefinding algorithms, the occurrence of backscatter with a power of >10 dB in the 15 km range gate channels of the radars has been quantified as a function of the offset in km between the location of the radar backscatter as determined by the SuperDARN rangefinding algorithms, and the known location of the high power beams at Tromsø and SPEAR. Figure 4 presents the results of such an analysis for column i) Hankasalmi-Tromsø in 1998; column ii) Þykkvibær-Tromsø in 1998; column iii) Þykkvibær-Tromsø in 2004; column iv) Hankasalmi-SPEAR in 2005; and column v) Þykkvibær-SPEAR in 2005. In this figure results are presented with the rangefinding algorithm used with a fixed pseudo-virtual height of 400 km (see Fig. 2), the standard assumption used in SuperDARN analysis, in row a), for the $\frac{1}{2}$-hop virtual height model of Chisham et al. (2008) in row (b) and for the $1\frac{1}{2}$-hop virtual height model of Chisham et al. (2008) in row (cii–cv). The ranges involved in Fig. 4 columns ii to v occur within the $\frac{1}{2}$-hop to $1\frac{1}{2}$-hop overlap region identified in Chisham et al. (2008), hence, the location of the scattering region is estimated using both models. In each panel backscatter occurrence is denoted on the left hand Y-axis labels. Also plotted is the actual location of the Tromsø and SPEAR field lines as a function of altitude, denoted on the right hand Y-axis label, taking into account the orientation of the geomagnetic field. In each panel the centre of the occurrence histogram is marked by a vertical dashed line, the irregularity height is marked by a horizontal dashed line, and the offset between the centre of the data occurrence histogram and the actual irregularity location on the SPEAR or Tromsø field line is highlighted with a horizontal red bar. The data in Figs. 4i and 4ii were presented in Yeoman et al. (2001), although in that case the actual irregularity height of 210 km was used, and the range offset was expressed in terms of latitude and longitude. Figure 4ai illustrates that the standard pseudo-virtual height assumption leads to a 45 km underestimate (expressed to an accuracy of the nearest 15 km range gate) of the backscatter range for the Hankasalmi-Tromsø $\frac{1}{2}$-hop propagation path, which has an elevation angle of 10° and a range of 825 km. As concluded in Yeoman et al. (2001), such propagation paths give an accurate ground range if the actual irregularity height is used. The $\frac{1}{2}$-hop virtual height model of Chisham et al. (2008) (Fig. 4bi) also

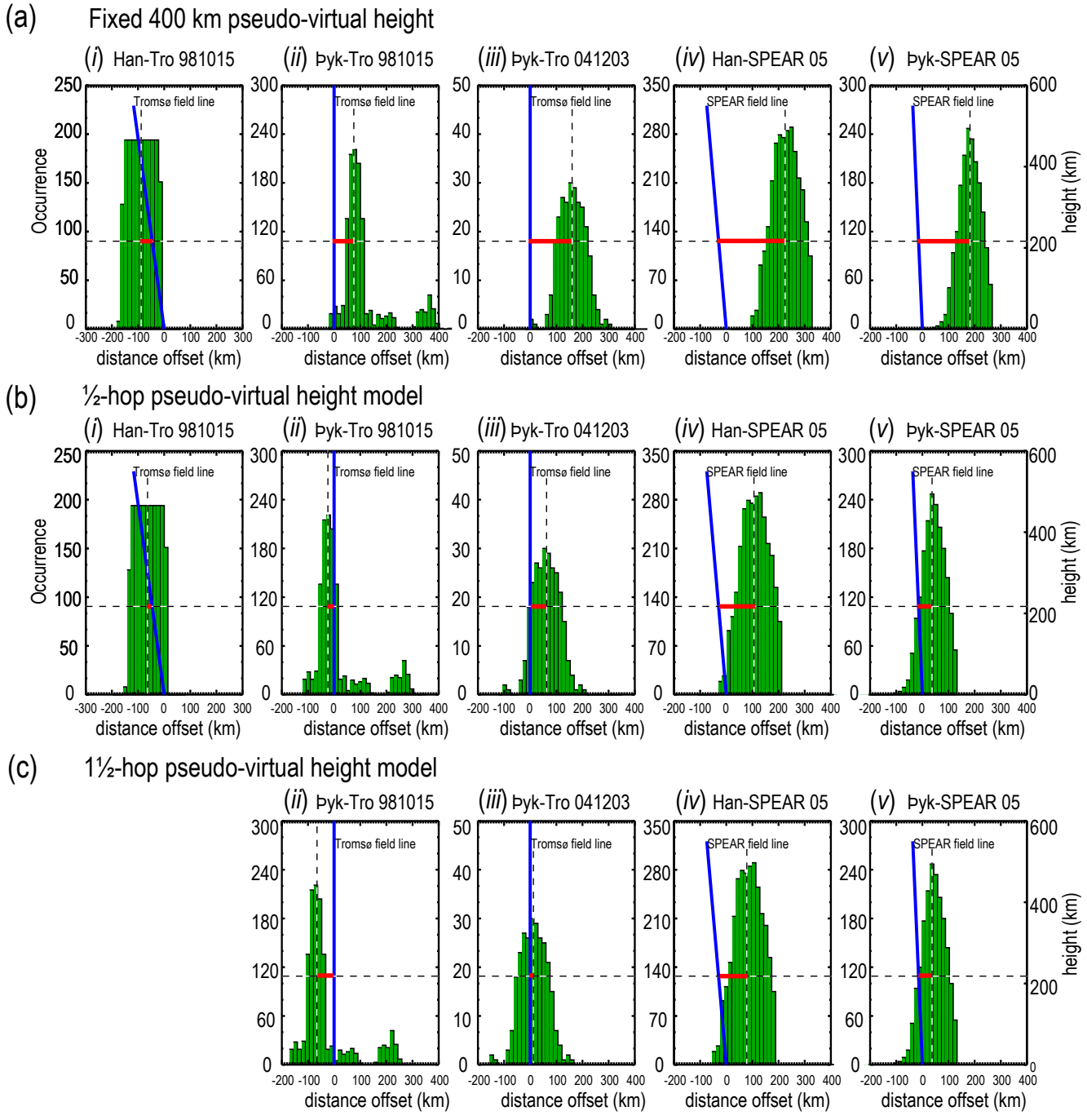

Fig. 4. Occurrence rates for artificial backscatter detection at a power of >10 dB for: column i) Hankasalmi-Tromsø in 1998 column ii) Þykkvibær-Tromsø in 1998; column iii) Þykkvibær-Tromsø in 2004; column iv) Hankasalmi-SPEAR in 2005; column v) Þykkvibær-SPEAR in 2005. Row **(a)** presents data using the standard SuperDARN virtual height model, row **(b)** presents the new $\frac{1}{2}$-hop virtual height model of Chisham et al. (2008), and row **(c)** presents the new $1\frac{1}{2}$-hop virtual height model of Chisham et al. (2008). In each panel the centre of the occurrence histogram is marked by a vertical dashed line, the irregularity height is marked by a horizontal dashed line, and the offset between the centre of the data occurrence histogram and the actual irregularity location on the SPEAR or Tromsø field line is highlighted with a horizontal red bar.

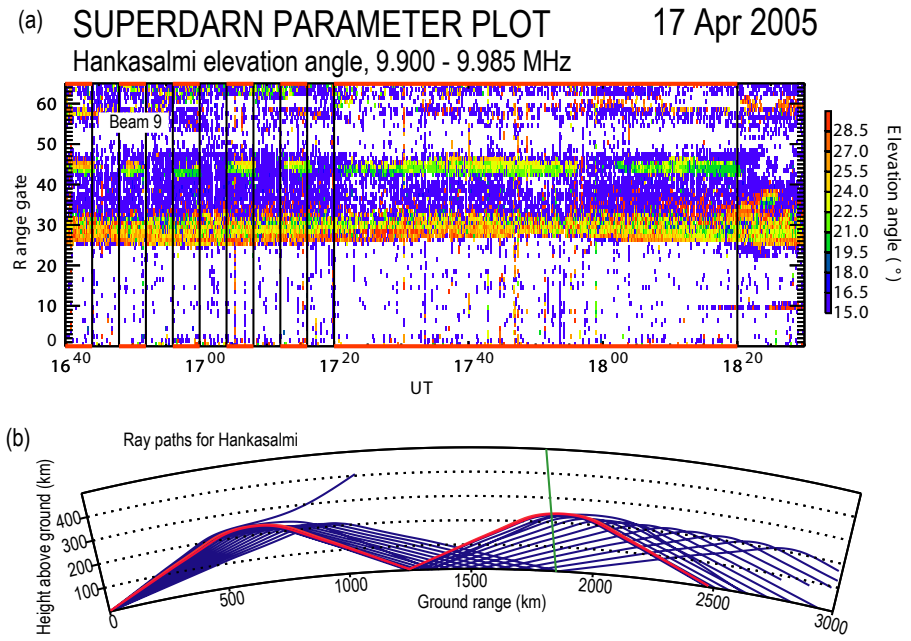

Fig. 5. **(a)** The elevation angle of the backscatter shown in Fig. 3, presented in the same format. **(b)** A raytrace of the HF propagation path for the transmission displayed in Fig. 3 and panel (a). The green line indicates the location of the field line intersecting the SPEAR location, whereas the red rays correspond to the elevation angles measured in panel (a).

offers an improvement over the standard algorithm, reducing the offset to just 15 km. Figure 4 row a) clearly shows that the standard 400 km pseudo-virtual height assumption leads to an overestimate of backscatter range for all the longer (probably $1\frac{1}{2}$-hop) propagation paths, as expected. Figure 4aii presents data from the Þykkvibær-Tromsø $1\frac{1}{2}$-hop (elevation angle 18°) and $2\frac{1}{2}$-hop (elevation angle 31°) paths. Again Yeoman et al. (2001) deduced that these paths produced a ground range offset of 115 km and 390 km respectively over a range of 1830 km if the actual irregularity heights were used. These offsets reduce to 75 km and 360 km, respectively, with a pseudo-virtual height assumption of 400 km (for clarity only the 75 km offset for the $1\frac{1}{2}$-hop propagation path is marked on the figure). In Fig. 4bii the $\frac{1}{2}$-hop virtual height model of Chisham et al. (2008) reduces this offset to 30 km, whereas in Fig. 4cii the $1\frac{1}{2}$-hop virtual height model produces an offset of 75 km. In both cases the range is now underestimated, rather than over-estimated. Figure 4aiii presents more recent data taken over the Þykkvibær-Tromsø $1\frac{1}{2}$-hop path in December 2004. The range offset can be seen to have increased significantly from the 1998 data, to some 150 km. In Fig. 4biii the $\frac{1}{2}$-hop virtual height model of Chisham et al. (2008) reduces this offset to 60 km, whereas in Fig. 4ciii the $1\frac{1}{2}$-hop virtual height model produces an offset of just 15 km. Data from the $1\frac{1}{2}$-hop Hankasalmi-SPEAR path (range 1890 km) and Þykkvibær-SPEAR path (range 2007 km) during 2004 and 2005 are presented in Fig. 4iv and 4v, respectively. These show similar larger range offsets of 270 km and 195 km for the 400 km fixed pseudo-virtual height calculation in Fig. 4aiv and 4av, respectively. In Fig. 4biv and 4bv the $\frac{1}{2}$-hop virtual height model of Chisham et al. (2008) reduces these offsets to 130 km and 60 km respectively, whereas in Fig. 4civ the $1\frac{1}{2}$-hop virtual height model reduces the offset for the Hankasalmi-SPEAR path further to 105 km. For the Þykkvibær-SPEAR path the $\frac{1}{2}$-hop and $1\frac{1}{2}$-hop virtual height model are essentially identical.

3.2 Elevation angle effects on rangefinding accuracy

Figure 5a presents data in the same format as Fig. 3, but here the elevation angle of arrival of the backscatter is presented. The elevation angles are seen to be consistent through the artificial backscatter patches, with elevation angles of 21°–23° typically being recorded. Figure 5b presents a raytrace (using code based on Jones and Stephenson, 1975) of the HF propagation path for the transmission displayed in Figs. 3 and 5a with rays shown for elevation angles 10–24° at 1° intervals. The raytrace is based on a double Chapman layer fitted to an EISCAT Svalbard radar electron density profile, scaled by data from the SPEAR ionosonde. The green line indicates the location of the field line intersecting the SPEAR location. The red rays correspond to the elevation angles measured in Fig. 5a. These rays, with elevation angles of 21°–22° are excellent candidates for being orthogonal to the magnetic field above SPEAR. Orthogonality is predicted to be achieved at an altitude of 200 km, which is in good agreement with the interaction height of the SPEAR beam as determined through

incoherent scatter measurements from the EISCAT Svalbard radar. Ground scatter is observed in Figs. 3 and 5a centred at range gate 28 (ranges of ∼1300 km), and this again is in good agreement with the raytrace; rays above 24° are expected to penetrate the ionosphere. In fact the ground and natural ionospheric backscatter observed at higher frequencies (13.3 MHz, not shown) are also in good agreement with raytracing through this model ionosphere.

As we now, for the first time, have a propagation path from Hankasalmi to both Tromsø on a $\frac{1}{2}$-hop path and SPEAR on a $1\frac{1}{2}$-hop path, it is possible to use the Tromsø heater as an accurate calibration point for the Hankasalmi elevation angle of arrival data, and then accurately establish the propagation path for $1\frac{1}{2}$-hop backscatter generated at SPEAR. This sheds light on the evaluation of the virtual height models presented in Sect. 3.1, and offers an alternative strategy for rangefinding corrections when reliable elevation angle data are available from SuperDARN. In Fig. 6a, the Hankasalmi range gates which record backscatter at powers greater than 10 dB induced by the SPEAR system during all available SPEAR experiments in 2004 and 2005, such as those illustrated in Fig. 3 are plotted against the corresponding elevation angle of arrival from the main array-interferometer array cross correlation such as those illustrated in Fig. 5a, where it is available. The angle of arrival data are binned into 1° bins, and occurrence is indicated by color contours. The line of best fit to this occurrence data is plotted as a solid black line, with the equation of the line included in the top left of the panel. The dotted black lines represent best fit lines to the occurrence distribution at ±1 standard deviation. The black filled circles represent the equivalent ranges calculated from the range offsets from the original study of the Þykkvibær-Tromsø $1\frac{1}{2}$- and $2\frac{1}{2}$-hop paths studied in Yeoman et al. (2001). A clear trend of increasing range gate with increasing elevation angle is observed, with the data from the Þykkvibær-Tromsø $1\frac{1}{2}$-hop path lying within the range of the lower elevation angle data recorded in 2004/05. The Þykkvibær-Tromsø $2\frac{1}{2}$-hop path produces a somewhat more extreme range error, as might be expected from such an unusual propagation path. These elevation angles will be compared to those employed in the development of the virtual height models of Chisham et al. (2008) in the next section.

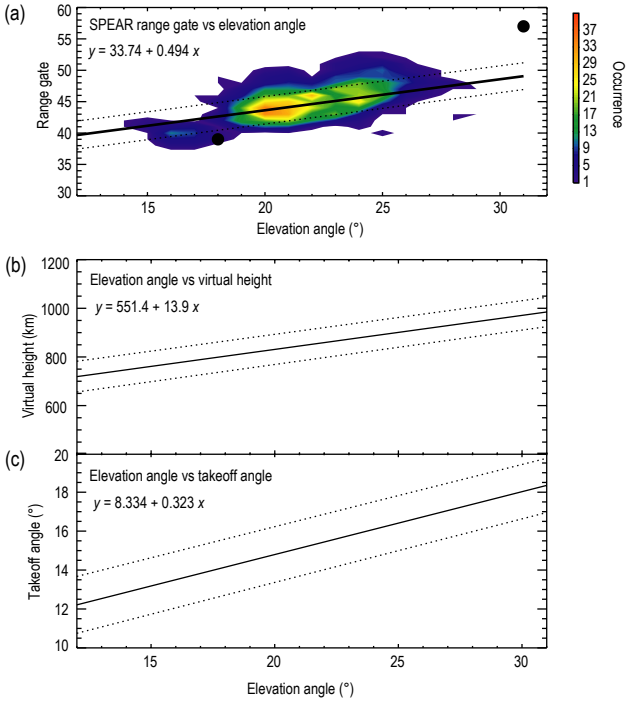

Fig. 6. (a) An occurrence plot of the range gate in which artificially-stimulated backscatter is induced in the Hankasalmi field of view vs. the elevation angle of the backscatter, for all backscatter observed by the Hankasalmi-SPEAR combination. The black dots represent previous data from the Þykkvibær-Tromsø experiments. See text for details. **(b)** Best fit lines for assumed irregularity pseudo-virtual height vs. measured elevation angle for the data presented in panel (a). The dotted lines represent ±1 standard deviation of the occurrence distribution. **(c)** As for (b), but for assumed takeoff angle vs. measured elevation angle.

4 Discussion

Artificial radar backscatter generated at a known ground range has been used to evaluate the standard SuperDARN rangefinding algorithm, and the new virtual height models presented by Chisham et al. (2008). The previous analysis of Yeoman et al. (2001) suggested that for $\frac{1}{2}$-hop backscatter, with typical elevation angles of ∼10°, the range accuracy is within one 15 km range gate if the actual irregularity altitude is used in the rangefinding algorithm. This analysis of a simple $\frac{1}{2}$-hop path was in accord with previous results, as detailed in Yeoman et al. (2001). The new virtual height model of Chisham et al. (2008) retains this good level of accuracy for short $\frac{1}{2}$-hop propagation paths.

Longer ranges are routinely accessed by SuperDARN radars via $1\frac{1}{2}$-hop paths, where the HF rays reflect from the ionosphere, and then scatter from the ground or sea surface, before reaching an ionospheric target, as depicted schematically in Fig. 2. The first analysis of range accuracy over such $1\frac{1}{2}$-hop propagation paths was also presented by Yeoman et al. (2001), who investigated a path with an elevation angle of ∼18° at a ground range of ∼1800 km, where the rangefinding algorithm had an offset of four 15 km range gates for the standard pseudo-virtual height assumption of 400 km. The analysis of a number of $1\frac{1}{2}$-hop propagation paths presented here demonstrates that the accuracy of the rangefinding algorithms is rather variable, but that the new pseudo-virtual height models of Chisham et al. (2008) consistently make a very significant improvement to the accuracy of SuperDARN rangefinding. Averaged over the 4 propagation paths presented in Fig. 4, the new virtual height models improve the

error in the rangefinding from 165 km when using the standard pseudo-virtual height assumption to just 60 km. For 3 out of the 4 propagation paths the new $1\frac{1}{2}$-hop propagation path pseudo-virtual height model gives a better correction than the $\frac{1}{2}$-hop propagation path pseudo-virtual height model. This is not surprising, given that the propagation paths used are most likely $1\frac{1}{2}$-hop. The $2\frac{1}{2}$-hop propagation path presented in Fig. 4ii is again improved when the new pseudo-virtual height model is employed, although the rangefinding accuracy is still poor. Such $2\frac{1}{2}$-hop paths are rarely observed in practice, although they could be important in the lower latitude SuperDARN radars such as that recently deployed at Wallops Island.

Some of the discrepancies between the actual and predicted ground ranges can be understood by considering the elevation angles of the observed backscatter, and the elevation angle data used in formulating the new pseudo-virtual height model. Ranges such as those for the Hankasalmi-Tromsø path are only available through $\frac{1}{2}$-hop propagation. The new virtual height model of Chisham et al. (2008) produces a slightly lower pseudo-virtual height than the conventional SuperDARN rangefinding algorithm at these ranges, and thus gives a small improvement in range accuracy over the standard algorithm. The data from the Saskatoon radar, which were used in the development of the new virtual height models, showed elevation angles of $\sim$18° dominated at these ranges (see Fig. 3 of Chisham et al., 2008). These elevation angles compare with elevation angles measured at Hankasalmi of 10° for the heater-induced scatter (see Yeoman et al., 2001). This reflects the difference between the typical altitudes of natural and heater-induced ionospheric irregularities. Using a pseudo-virtual height closer to the actual irregularity height offers a further improvement, but the range accuracy is satisfactory in either case. The longest propagation paths examined here, those to SPEAR, give essentially the same range result for the $\frac{1}{2}$-hop and $1\frac{1}{2}$-hop models. Typical $1\frac{1}{2}$-hop elevation angles to these ranges as used by Chisham et al. (2008) are $\sim$22°, in close agreement with those measured for the heater-induced scatter as presented in Fig. 5. Figure 6a has demonstrated that, for a given propagation path, the range gate of the observed data increases systematically with the elevation angle of the backscatter, thus we expect higher elevation angle backscatter to require a larger range correction, or a higher pseudo-virtual height. A significant improvement in range accuracy is produced by both new virtual height models for these paths, although both still produce a consistent offset, placing the backscatter farther from the radar than its actual location, implying that the actual propagation paths often have elevation angles in excess of those used in developing the models of Chisham et al. (2008). The Þykkvibær-Tromsø path (a 1830 km, $1\frac{1}{2}$-hop path) produces significant differences in range between the $\frac{1}{2}$-hop and $1\frac{1}{2}$-hop models. Older data on this path from 1998 (Fig. 4ii) had measured elevation angles of 18°, whereas the Saskatoon data which were used in the development of the new virtual height models showed elevation angles of 14° dominated at these ranges, on a $\frac{1}{2}$-hop propagation path (see Fig. 3 of Chisham et al., 2008). No significant $1\frac{1}{2}$-hop propagation paths were observed for these ranges at Saskatoon. The relatively low altitude of the heater-induced scatter makes a $1\frac{1}{2}$-hop path preferential for artificial scatter at these ranges, whereas the natural scatter from Saskatoon in Chisham et al. (2008) is from a $\frac{1}{2}$-hop path. The $1\frac{1}{2}$-hop virtual height model of Chisham et al. (2008) was extrapolated into these ranges, and would represent high elevation angle scatter. This leads to the new $1\frac{1}{2}$-hop virtual height model underestimating the ground range of this 18° elevation angle scatter, whereas the $\frac{1}{2}$-hop model is accurate to 30 km. The more recent data (from 2004, Fig. 4iii) have a larger range offset, resulting from higher elevation angles, and for these data the $1\frac{1}{2}$-hop virtual height model gives the more accurate ground ranges.

The difference in range accuracy between the recent data from the two $1\frac{1}{2}$-hop propagation paths to SPEAR, (270 and 195 km in Figs. 4aiv and 4av) compared to the older results from Yeoman et al. (2001) (75 km in Fig. 4aii) deserves some further comment. The 75 km offset was reported to be very consistent in the data presented in Yeoman et al. (2001) who concluded that the determination of the location of the backscatter was only weakly controlled by variations in the ionosphere between the radar and target ionosphere during the era when the original experiments were performed. Some of the differences between the Yeoman et al. (2001) data and the new data presented here can most likely be attributed to path geometry, but the increase in range error between the Þykkvibær-Tromsø path in 1998 (Fig. 4ii) and the same path recorded in 2004 (Fig. 4iii) suggests that the solar cycle is playing a role, as the radar operating frequency was similar in all cases. For the 1998 data the 3 month averaged sunspot number was 75 (63% of the cycle 23 maximum) whereas it was 30 in 2005 (25% of the cycle 23 maximum). Solar cycle and season will have a strong effect on the overlying F region critical frequency (*fo*F2) of the ionosphere through which the SuperDARN HF rays propagate. A ray of the same elevation angle and frequency will refract at a higher altitude (and hence a farther range) when *fo*F2 is lower, which in general will be at solar minimum compared to solar maximum. Solar minimum conditions might also be expected to increase the likelihood of the rays penetrating the ionosphere, thus preventing the measurement of artificial backscatter, although the success rate of such experiments does not appear to be significantly solar cycle dependent. To allow for a propagation path to the same location the elevation angle must increase at times of reduced *fo*F2. It thus seems likely that the level of solar activity plays a role in determining the viable $1\frac{1}{2}$-hop propagation path characteristics. Figure 6a suggests that the likely radar elevation angles for $1\frac{1}{2}$-hop backscatter have significantly increased as solar activity has decreased.

The data presented in Fig. 6a allow for a direct translation between the appropriate pseudo-virtual height input to the SuperDARN rangefinding algorithm and the elevation angle measured by the radar, as the rangefinding algorithm yields a range gate for each assumed pseudo-virtual height for a fixed ground range location. Such a plot is presented in Fig. 6b, which presents assumed pseudo-virtual height against elevation angle, such that the rangefinding algorithm places the appropriate range gate at the correct ground range. The solid line uses the best fit line from Fig. 6a in this calculation, whereas the dashed lines use the corresponding ± 1 standard deviation lines. The equation of the solid line is given in the upper left corner of the graph. An alternative approach to providing a pseudo-virtual height to the SuperDARN rangefinding algorithm is to provide an assumed take-off angle for the ray, based on straight-line propagation to the pseudo-virtual height (see Fig. 2). This can similarly be combined with the range gate vs. elevation angle data from the Hankasalmi-SPEAR path to provide a correction factor which places the data at the correct ground range, and such a plot is presented in Fig. 6c, in the same format as Fig. 6b.

5 Summary

Artificial coherent HF radar backscatter generated by ionospheric heating facilities have provided a high power signature at a known ground range which has been used to evaluate the standard rangefinding algorithm of the SuperDARN radar facilities, and the new virtual height models presented by Chisham et al. (2008). The results have highlighted significant issues with the accuracy of the standard SuperDARN rangefinding algorithm. These issues may be largely mitigated through the use of the new virtual height models which allow backscatter location to an average accuracy of ± 60 km for $1\frac{1}{2}$-hop paths. In addition, direct use of the measured elevation angle of arrival provides a new method of determining the backscatter location to an accuracy of ± 45 km for $1\frac{1}{2}$-hop paths with elevation angles in the range 10°–30° for SuperDARN data recorded at ranges 1500–2500 km, where reliable elevation angle data exist.

Acknowledgements. We thank the director and staff of EISCAT for the operation of the Tromsø heater facility. The SPEAR, Hankasalmi and Þykkvibær facilities are deployed and operated by the University of Leicester, and funded by the STFC.

Editor in Chief W. Kofman thanks A. V. Koustov and J. M. Ruohoniemi for their help in evaluating this paper.

References

André, R., Hanuise, C., Villain, J.-P., and Cerisier, J.-C.: HF radars: multifrequency study of refraction effects and localization of scattering, Radio Sci., 32, 153–168, 1997.

Baker, K. B., Greenwald, R. A., Walker, A. D. M., Bythrow, P. F., Zanetti, L. J., Potemra, T. A., Hardy, D. A., Rich, F. J., and Rino, C. L.: A case study of plasma processes in the dayside cleft, J. Geophys. Res., 91, 3130–3144, 1986.

Blanchard G. T., Ellington, C. L., and Baker, K. B.: Comparison of dayside magnetic separatrix signatures in HF and incoherent scatter radar data, J. Geophys. Res., 108, 1456, doi:10.1029/2003JA009910, 2003.

Chisham, G., Freeman, M. P., Lam, M. M., Abel, G. A., Sotirelis, T., Greenwald, R. A., and Lester, M.: A statistical comparison of SuperDARN spectral width boundaries and DMSP particle precipitation boundaries in the afternoon sector ionosphere, Ann. Geophys., 23, 3645–3654, 2005, http://www.ann-geophys.net/23/3645/2005/.

Chisham, G., Lester, M., Milan, S. E., Freeman, M. P., Bristow, W. A., Grocott, A., McWilliams, K. A., Ruohoniemi, J. M., Yeoman, T. K., Dyson, P. L., Greenwald, R. A., Kikuchi, T., Pinnock, M., Rash, J. P. S., Sato, N., Sofko, G. J., Villain, J.-P., and Walker, A. D. M.: A decade of the Super Dual Auroral Radar Network (SuperDARN): scientific achievements, new techniques and future directions, Surv. Geophys., 28, 33–109, 2007.

Chisham, G., Yeoman, T. K., and Sofko, G. J.: Mapping ionospheric backscatter measured by the SuperDARN HF radars – Part 1: A new empirical virtual height model, Ann. Geophys., 26, 823–841, 2008, http://www.ann-geophys.net/26/823/2008/.

Greenwald, R. A., Baker, K. B., Dudeney, J. R., Pinnock, M., Jones, T. B., Thomas, E. C., Villain, J.-P., Cerisier, J. C., Senior, C., Hanuise, C., Hunsucker, R. D., Sofko, G., Koehler, J., Nielsen, E., Pellinen, R., Walker, A. D. M., Sato, N., and Yamagishi, H.: DARN/SUPERDARN A global view of the dynamics of high-latitude convection, Space Sci. Rev., 71, 761–796, 1995.

Jones, R. M. and Stephenson, J. J.: A Versatile Three-Dimensional Ray Tracing Computer Program for Radio Waves in the Ionosphere, Office of Telecommunications, OT 75–76, US Department of Commerce, Washington, USA, 1975.

Lockwood, M., Lanchester, B. S., Frey, H. U., Throp, K., Morley, S. K., Milan, S. E., and Lester, M.: IMF control of cusp proton emission intensity and dayside convection: implications for component and anti-parallel reconnection, Ann. Geophys., 21, 955–982, 2003, http://www.ann-geophys.net/21/955/2003/.

McWilliams, K. A., Sofko, G. J., Yeoman, T. K., Milan, S. E., Sibeck, D. G., Nagai, T., Mukai, T., Coleman, I. J., Hori, T., and Rich, F. J.: Simultaneous observations of magnetopause flux transfer events and of their associated signatures at ionospheric altitudes, Ann. Geophys., 22, 2181–2199, 2004, http://www.ann-geophys.net/22/2181/2004/.

Pinnock, M., Rodger, A. S., Dudeney, J. R., Rich, F., and Baker, K. B.: High spatial and temporal resolution observations of the ionospheric cusp, Ann. Geophys., 13, 919–925, 1995, http://www.ann-geophys.net/13/919/1995/.

Rietveld, M. T., Kohl, H., Kopka, H., and Stubbe, P.: Introduction to ionospheric heating at Tromsø – I. Experimental overview, J. Atmos. Terr. Phys., 55, 577–599, 1993.

Robinson, T. R.: The heating of the high latitude ionosphere by high power radio waves, Phys. Rep., 179, 79–209, 1989.

Robinson, T. R., Stocker, A. J., Bond, G. E., Eglitis, P., Wright, D. M., and Jones, T. B.: O- and X-mode heating effects observed simultaneously with the CUTLASS and EISCAT radars and low power HF diagnostics at Tromsø, Ann. Geophys., 15, 134–136,

1997,
http://www.ann-geophys.net/15/134/1997/.

Robinson, T. R., Yeoman, T. K., Dhillon, R. S., Lester, M., Thomas, E. C., Thornhill, J. D., Wright, D. M., van Eyken, A. P., and McCrea, I. W.: First observations of SPEAR induced artificial backscatter from CUTLASS and the EISCAT Svalbard radars, Ann. Geophys., 24, 291–309, 2006,
http://www.ann-geophys.net/24/291/2006/.

Ruohoniemi, J. M., Greenwald, R. A., Baker, K. B., Villain, J.-P., and McCready, M. A.: Drift motions of small-scale irregularities in the high latitude F region: an experimental comparison with plasma drift motions, J. Geophys. Res., 92, 4553–4564, 1987.

Sandholt, P. E., Farrugia, C. J., Stauning, P., Cowley, S. W. H., and Hansen, T.: Cusp/cleft auroral forms and activities in relation to ionospheric convection: Responses to specific changes in solar wind and interplanetary magnetic field conditions, J. Geophys. Res., 101, 5003–5020, 1996.

Senior, A., Borisov, N. D., Kosch, M. J., Yeoman, T. K., Honary, F., and Rietveld, M. T.: Multi-frequency HF radar measurements of artificial F-region field-aligned irregularities, Ann. Geophys., 22, 3503–3511, 2004,
http://www.ann-geophys.net/22/3503/2004/.

Sotirelis, T., Ruohoniemi, J. M., Barnes, R. J., Newell, P. T., Greenwald, R. A., Skura, J. P., and Meng, C. I.: Comparison of SuperDARN radar boundaries with DMSP particle precipitation boundaries, J. Geophys. Res., 110, A06302, doi:10.1029/2004JA010732, 2005.

Villain, J.-P., Greenwald, R. A., and Vickrey, J. F.: HF ray-tracing at high latitude using measured meridional electron density distributions, Radio Sci., 19, 359–374, 1984.

Wright, D. M., Davies, J. A., Robinson, T. R., Chapman, P. J., Yeoman, T. K., Thomas, E. C., Lester, M., Cowley, S. W. H., Stocker, A. J., Horne, R. B., and Honary, F.: Space Plasma Exploration by Active Radar (SPEAR): an overview of a future radar facility, Ann. Geophys., 18, 1248–1255, 2000,
http://www.ann-geophys.net/18/1248/2000/.

Yeoman, T. K., Lester, M., Cowley, S. W. H., Milan, S. E., Moen, J., and Sandholt, P. E.: Simultaneous observations of the cusp in optical, DMSP and HF radar data, Geophys. Res. Lett., 24, 2251–2254, 1997a.

Yeoman, T. K., Wright, D. M., Robinson, T. R., Davies, J. A., and Rietveld, M. T.: High spatial and temporal resolution observations of an impulse-driven field line resonance in radar backscatter artificially generated with the Tromsø heater, Ann. Geophys., 15, 634–644, 1997b,
http://www.ann-geophys.net/15/634/1997/.

Yeoman, T. K., Wright, D. M., Stocker, A. J., and Jones, T. B.: An evaluation of range accuracy in the SuperDARN over-the-horizon HF radar systems, Radio Sci., 36, 801–813, 2001.